

Article

Performance Improvement of Human Centrifuge Systems through Multi-Objective Configurational Design Optimisation

Asher Winter , Navid Mohajer, Darius Nahavandi and Shady Mohamed

Institute for Intelligent Systems Research and Innovation (IISRI), Deakin University, Waurn Ponds, Geelong 3216, Australia

* Correspondence: a.winter@deakin.edu.au

Abstract: Human Centrifuge Systems (HCSs) are an effective training tool to improve the G-acceleration and Spatial Disorientation (SD) tolerance of aircrew. Though highly capable HCSs are available, their structure and performance are yet to be fully optimised to efficiently recreate the G-vectors produced using Aircraft Combat Manoeuvres (ACMs). To achieve this improvement, the relationship between configurational design and HCS performance should be profoundly investigated. This work proposes a framework for identifying the optimal configurational design of an active four Degree-of-Freedom (DoF) HCS. The relationship between configurational design parameters and objective criteria is established using inverse kinematics and dynamics. Then, a multi-objective evolutionary optimiser is used to identify the optimum arm length and seat position, minimising the Coriolis effect, relative acceleration ratio, and cost. The results of the work show that the applied optimisation step can significantly contribute to (1) efficiently replicating the aircraft motion, (2) minimising the detrimental effects generated during HCS motion, and (3) reducing the overall cost of the system. The applied methodology can be adapted to HCSs with different structures and DoFs.

Keywords: Human Centrifuge System; multi-objective optimisation; configurational design; inverse kinematics and dynamics



Citation: Winter, A.; Mohajer, N.; Nahavandi, D.; Mohamed, S. Performance Improvement of Human Centrifuge Systems through Multi-Objective Configurational Design Optimisation. *Aerospace* **2023**, *10*, 1013. <https://doi.org/10.3390/aerospace10121013>

Academic Editor: Gokhan Inalhan

Received: 18 October 2023

Revised: 16 November 2023

Accepted: 28 November 2023

Published: 2 December 2023



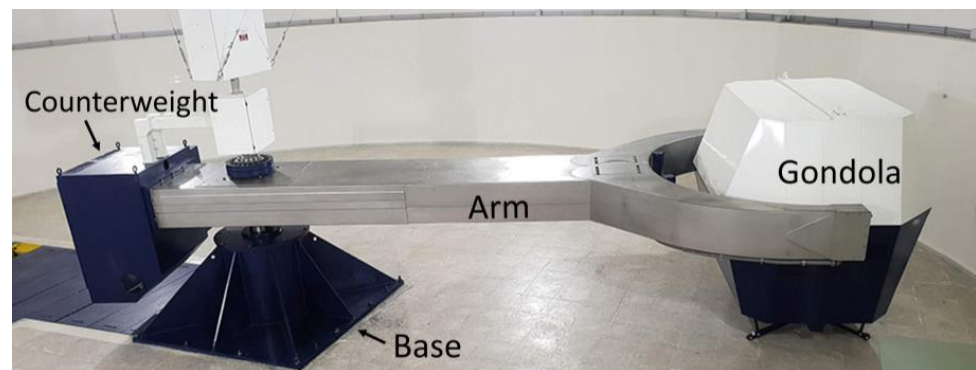
Copyright: © 2023 by the authors. Licensee MDPI, Basel, Switzerland. This article is an open access article distributed under the terms and conditions of the Creative Commons Attribution (CC BY) license (<https://creativecommons.org/licenses/by/4.0/>).

1. Introduction

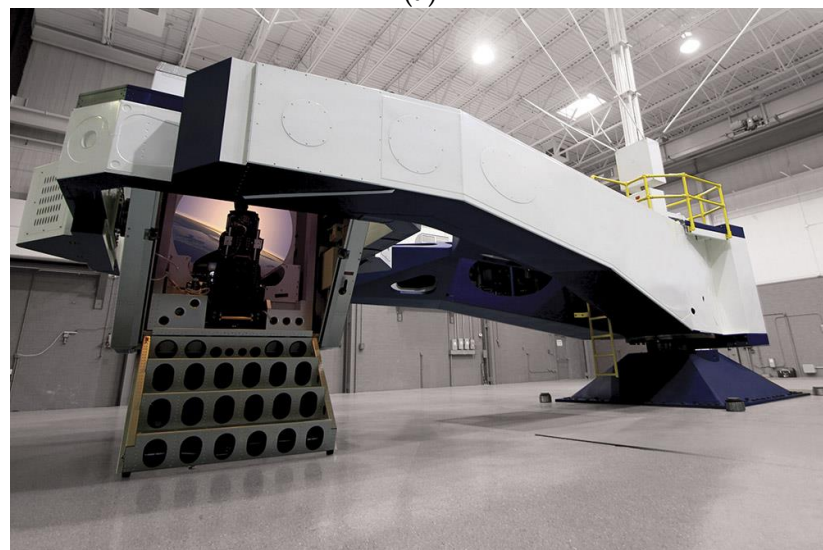
Human Centrifuge Systems (HCSs) are a critical motion platform for generating high G-accelerations akin to aircraft and spacecraft. The primary applications of HCSs include high G-acceleration and Spatial Disorientation (SD) training, medical research, and structure performance evaluation [1–3]. HCSs do not have a specific universal design or motion capability. However, the majority of HCSs consist of an arm that horizontally rotates about the system base, a gondola attached to the end of the arm with roll and pitch rotation, and a counterweight attached to the opposite side of the arm to offset the mass of the arm and gondola (Figure 1) [4–7]. The end-effector of an HCS is typically the head or chest of the HCS user.

HCSs generate the desired G-acceleration at the end-effector through rotation of the arm and gondola. Arm rotation generates centripetal and tangential acceleration at the end-effector. The rotation of the gondola reorients the end-effector and transfers the generated accelerations along the desired body axes of the end-effector. NATO developed a standardisation agreement for high G-acceleration aircrew training, which can also be used to set minimum performance criteria for HCSs [8]. Based on the standardisation agreement, HCSs should be able to generate more than 9 G sustained and a minimum onset rate of 3 G/s. Current HCSs have G-acceleration capabilities ranging from 3 to 30 G and onset rate capabilities ranging from 5 to 15 G/s. HCSs can typically provide Open Loop (OL) and dynamic motion control modes. OL motion control, which is specified as Predefined Scenario Simulation (PSS) within this study, consists of pre-set motion profiles that enable repetition of specific motion scenarios [9]. Dynamic motion control is

generally defined as Dynamic Flight Simulation (DFS) and provides the HCS user with active control over HCS motion.



(a)



(b)

Figure 1. Two examples of operational HCSs: (a) G-lab [10] and (b) ATFS-400-25 [11].

The design and motion of standard HCSs produce several issues that inhibit high G-acceleration training. These issues include (1) HCS motion-induced Coriolis effect and differing blood pressure between the head and feet of the HCS user [7,12], (2) delayed response of HCS motion to given motion inputs due to inertia and limitations of HCS motors [13], and (3) accurate replication of the multi-axis G-acceleration of aircraft motion [14]. This study investigates the minimisation of these issues through optimisation of the configurational design of an HCS.

The main limiting factor of HCSs for DFS and aircraft motion simulation is Coriolis [12]. Coriolis is caused by differences in the angular acceleration vector between points of a body and can be induced on a user passively (from aircraft or HCS gondola movement) or actively (from user head movement) [15]. Coriolis is an undesirable effect on the aircrew as it can cause a conflict in information regarding body orientation and motion. This may result in symptoms such as motion sickness, nausea, and disorientation [15]. Within HCS motion, Coriolis is generated at the user's vestibular system during simultaneous rotation of the gondola or during user head movement. The detrimental effects of Coriolis are more severe in HCSs compared to aircraft, since the generated Coriolis is significantly larger than the Coriolis generated via aircraft motion [7,16]. This is mainly due to the gondola's short radius of rotation compared to an aircraft's turn radius.

Feet-to-Head Acceleration Ratio (FHAR) is the ratio of acceleration experienced at a person's feet relative to the head. The difference in feet and head acceleration is

predominantly caused via gondola roll rotation, which causes the user's feet to move farther away from the arm's Centre of Rotation (CoR) compared to the user's head. The magnitude of the difference between foot and head acceleration is inversely proportional to HCS arm length [7]. Higher values of FHAR can adversely affect blood perfusion and produce a higher pressure difference in the cardiovascular system between the feet and head [7]. As FHAR increases, blood pressure increases at the feet and drops at the head [7], resulting in blood pooling at the feet and poor circulation. The difference in pressure between body parts and the increase in vascular transmural pressure can result in harmful physiological effects such as arm pain and foot pain [1,17–20]. Mitigation of such physiological effects has been investigated through the implementation of guidance and anti-G equipment [17,18,21–23].

Within HCSs, physiological effects can occur with greater intensity [7,16]. However, the application of an optimal configurational design for a HCS could potentially reduce the increased magnitude of these effects. Minimising Coriolis and FHAR will improve HCS replication of aircraft motion in addition to improving user experience and reducing detrimental physiological effects. Longer arm lengths have been investigated to minimise Coriolis and FHAR; however, they may be considered impractical due to the increase in cost and torque requirements outweighing the minor reduction in Coriolis and FHAR [7]. Instead, altering gondola orientation and applying a motion controller have been observed to be more optimal methods for reducing Coriolis and FHAR [7,12,24]. These methods, however, cannot mitigate Coriolis actively induced by human movement [7,12].

HCS motion criteria require a durable HCS structure that can sustain the large forces imposed on it during high G-accelerations. Therefore, HCSs require the highest level of structural integrity, which presents numerous structural problems [25]. Increasing structural stability and durability is an easy task when weight is not an issue. However, due to actuator torque limits and motion requirements, HCSs need to be as light as possible, which results in design compromises for motor selection, structure strength, mass, and mass distribution [14]. Thus, it is difficult to develop an HCS that can generate accelerations and onset rates at the level of fidelity required for training profiles and replication of Aircraft Combat Manoeuvres (ACMs). HCSs predominantly consist of a high-cost structure with high maintenance conditions [6].

The majority of HCSs in operation globally have three Degrees of Freedom (DoFs), which include arm rotation, gondola roll rotation, and gondola pitch rotation. Research has primarily focused on the performance improvement of three-DoF HCSs [14,23,26–31]. However, research has concluded that HCSs with gondola roll, pitch, and yaw rotation can simulate aircraft motion more accurately and further reduce undesirable effects [9,16]. Motion simulators with six DoFs and high Range of Motion (RoM), such as Desdemona and Kraken, have been regarded as highly suitable for DFS and SD training [32,33]. These systems, however, do not have the G-acceleration and onset rate capabilities required for high G-acceleration training.

Validation of the HCS capability to generate the desired G-acceleration is typically focused on generating a G_z-acceleration profile with little to no consideration of acceleration generated along the x and y axes of the end-effector [6,14,27,28,34]. This is due to G_z-acceleration being the primary cause of the detrimental physiological effects experienced by the aircrew during high-G flight [17,35]. Research into the development and control of three-DoF HCSs has produced systems capable of generating desired G_z-acceleration profiles with maximum errors of 0.2 G in [27], 0.46 G in [36], 0.47 G in [28], 0.38 G to 0.5 G in [14], and 0.49 G, which is described as a very good result in [37]. These results from the simulation of G_z-acceleration profiles have been reported to verify the kinematic algorithms and control system design of three-DoF HCSs. However, such tracking errors are not ideal for an accurate simulation of ACMs.

1.1. HCS Configurational Design

Configurational design optimisation in this study consists of changing configurable kinematic parameters of a system to minimise or maximise certain aspects of the system. Multi-objective optimisation consists of changing one or more parameters to minimise or maximise multiple aspects of a system [38–40]. Rather than offering a single optimal solution, the results of multi-objective design optimisation of a system typically consist of Pareto sets that present the trade-offs between various solutions, with which one can discern for themselves what would be most optimal for their situation [41]. The current study investigates the minimisation of undesirable motion effects and system cost through optimising the configurable kinematic parameters of a HCS that affect the system's performance. Configurational design parameters of HCSs that affect motion, motion effects at the end-effector, G-acceleration output, and system cost include arm length, DoF of the system, RoM of gondola axes, gondola seat position, counterweight position, the masses of HCS components, and the performance criteria of the drive motors. The design parameters and their relationship to HCS performance will be briefly highlighted within this section.

Current HCS arm lengths range from 5 m to 18 m, with the mean arm length being approximately 8 m. The dominant reason for shorter arm lengths is cost. Longer arm lengths are pursued as they reduce the arm RPM required to generate the desired high G-accelerations and reduce the relative change in end-effector distance from the arm CoR during gondola rotation. Lower RPM reduces undesirable effects on the vestibular system caused by the planetary rotation of the gondola about the HCS base [42,43]. Lower RPM also reduces the magnitude of Coriolis acceleration generated at the end-effector. A reduction in the relative change in end-effector distance from the arm CoR reduces the difference between the feet and head acceleration of the HCS user [7].

The DoFs of a HCS have a significant impact on the motion capabilities of the system. The primary DoFs of HCSs are arm rotation about the base vertical axis and gondola roll rotation. Arm rotation generates the magnitude of the desired G-acceleration at the end-effector. Gondola roll rotation redirects centripetal acceleration along the z-axis of the end-effector. Several HCSs currently in operation have only these two DoFs [6,44]. Gondola pitch rotation enhances HCS generation of multi-axis G-accelerations through increasing gondola rotation capability to redirect tangential and gravitational acceleration. Research on HCSs and motion platforms with three-axis gondola rotation has shown that the addition of gondola yaw rotation can potentially improve HCS capability to redirect centripetal, tangential, and gravitational acceleration along the desired axes of the end-effector and enhance HCS capability in the generation of multi-axis G-acceleration profiles [9,16,45–48].

The RoM of the gondola rotation axes also greatly impacts the performance capabilities of a HCS, in addition to being critical values for the identification of the required motor performance criteria. Kraken and Desdemona are two highly capable motion platforms with continuous gondola rotation. This enables the systems to provide comprehensive motion for space, flight, and driving simulation. Smaller pitch and yaw RoM are greatly desired from a motor capability and HCS structure perspective, as they contribute to the cost and complexity of the system.

Seat position and orientation relative to HCS motion influence how the generated G-acceleration vectors affect the user. Within aircraft, seat reclination impacts the experienced G-acceleration and improves aircrew G-tolerance through redirecting the generated G-accelerations proportionally more along the body x-axis of the aircrew rather than the z-axis. This reduces the load on the cardiovascular system to perfuse blood to the head. Studies have shown that leaning the seat backwards can slightly increase G-tolerance [31,49]. According to such research, seat backrest angles ranging from 13 deg to 30 deg are implemented in fighter aircraft such as the F-35 and F-16 [50]. Seat position within the HCS gondola can typically be adjusted to situate the end-effector at the desired position relative to the gondola CoR.

Generally, a large mass of metal is used as the HCS counterweight. The configurational parameters of the counterweight include mass and distance from the arm CoR. A recent study, however, presented a novel approach in which the arm motor is used as the counterweight, thus removing the need for and cost of the mass of metal [6]. The same approach could be used in future developments of HCSs, with an additional counterweight added only if the arm motor does not have substantial mass.

1.2. Paper Contributions

The optimisation of HCSs to more accurately replicate aircraft motion and minimise undesired forces and effects has predominantly focused on improving operational parameters, the Inverse Kinematic and Dynamic (IKD) analysis method, and the control algorithm of three-DoF HCSs [7,12,14,26,30,51,52]. To the best of our knowledge, the investigation of a four-DoF HCS and configurational design optimisation of the system to mitigate Coriolis, FHAR, and cost has not been performed nor received much attention within published research [6,7,16,24]. The contribution of this work is the investigation of HCS performance optimisation through optimising the configurational design parameters of a four-DoF HCS. Such systems are not typically used for high G-acceleration training but rather as SD training platforms, e.g., the GYROLAB series [45]. Thus, our study investigates the addition of gondola yaw rotation and the multi-objective optimisation of the arm length and seat position of a four-DoF HCS to minimise Coriolis, FHAR, and cost. Additionally, the required RoM of the gondola motors will be identified. HCS optimisation will be implemented using an efficient MATLAB global multi-objective optimisation solver. The tracking error of the HCS replication of three ACMs will also be analysed to ensure that the optimised design parameters do not inhibit the accurate replication of multi-axis G-accelerations.

The rest of this paper is organised in seven sections. Section 2 presents the IKD analysis for a four-DoF HCS. Section 3 discusses the problem formulation and presents the correlation between HCS configurational design parameters and Coriolis, FHAR, and cost. Section 4 presents the multi-objective optimisation methodology used to enhance HCS performance. Section 5 presents the optimisation results and observations. Section 6 provides discussion on the results and optimisation method. Section 7 discusses future developments of the study. Finally, Section 8 presents the conclusions of the work.

2. Kinematic and Dynamic Model of a Four-Axis Human Centrifuge System

This study aims to optimise the performance characteristics of a four-DoF HCS through optimisation of the configurational design of the HCS. A four-DoF HCS is selected due to research concluding that such systems are more capable of producing the multi-axis G-acceleration of ACMs [9,16]. To achieve this aim, the kinematic and dynamic motion of the HCS need to be first identified. This section presents the IKD analysis for a four-DoF HCS. The four active DoF consist of (1) arm rotation about the base's vertical z-axis, (2) gondola roll rotation, (3) gondola pitch rotation, and (4) gondola yaw rotation. The initial orientation of the gondola (link 4) body frame (BF) has the x-axis aligned horizontally perpendicular to the arm, the y-axis aligned parallel with the arm, and the z-axis aligned vertically (Figure 2). The Centre of Mass (CoM) of the HCS user's chest within the gondola is treated as the end-effector. The desired G-acceleration vector generated at the HCS end-effector is assumed to be known for this analysis and ideally would consist of inflight data of the G-accelerations experienced at the CoM of the pilot's chest during the performance of ACMs. From the known G-acceleration vector output, HCS kinematic and dynamic parameters can be calculated using IKD. The IKD model of the HCS is obtained using an IKD analysis adopted from [7].

The gondola seat is localised within the gondola with respect to the gondola BF. If the seat position $(\mathbf{p}_{\text{seat}}) = [0 \ 0 \ 0]^T$, the seat is located at the intersection of the gondola's three rotation axes. It is assumed that all three gondola rotation axes intersect at the gondola CoM. It is assumed that the Seat Reference Frame (SRF) is located at the centre of

the intersection of the seat base and back (Figure 3). This location of the SRF removes the need to recalculate the displacement of the user’s body for different seat sizes.

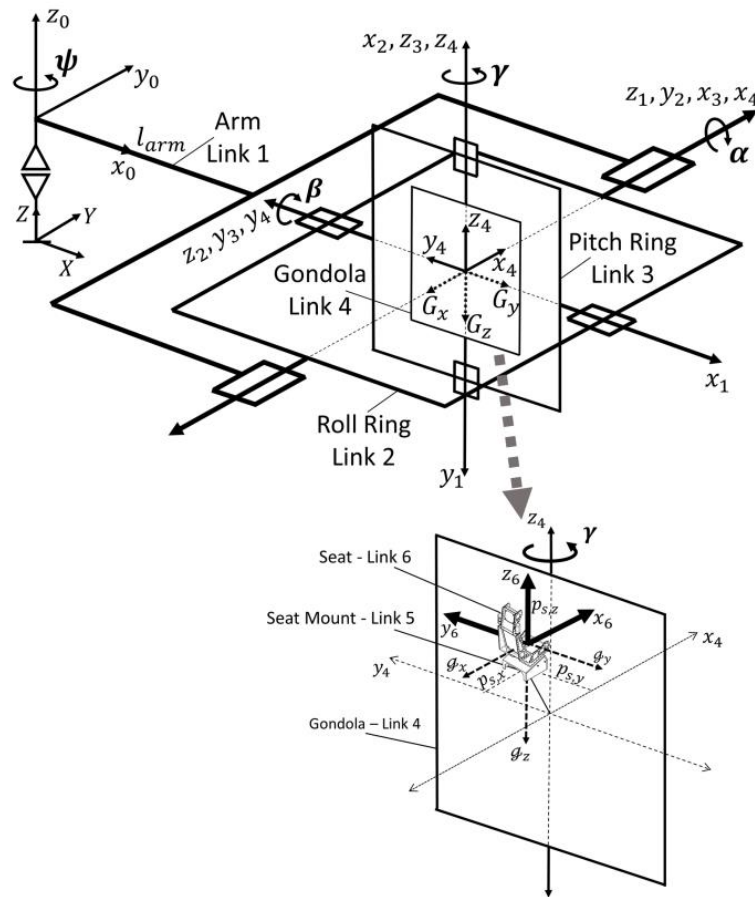


Figure 2. Coordinate frames for a four-axis Human Centrifuge System.

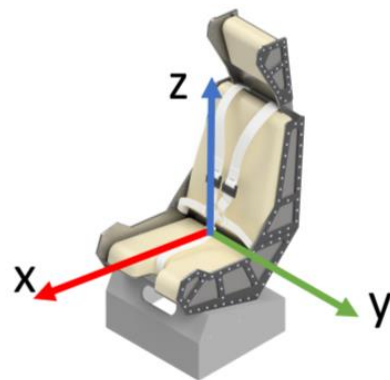


Figure 3. Gondola seat reference frame.

2.1. Inverse Kinematic Analysis

The primary HCS kinematics to be determined are arm angular velocity and acceleration and gondola roll, pitch, and yaw rotation angles. These kinematic parameters are to be expressed with respect to the Inertial Frame (IF) (X, Y, Z). The known HCS G-acceleration vector output at the gondola a_{gon} can be expressed in the IF using the rotational transformation matrix R .

$$a = Ra_{gon} \tag{1}$$

where \mathbf{a} is the HCS G-acceleration vector expressed in the IF. For arm rotation angle $\psi = 0$, \mathbf{R} can be defined by successive gondola yaw, pitch, and roll rotation in the IF.

$$\mathbf{R} = \begin{bmatrix} c\beta c\gamma & -c\beta s\gamma & s\beta \\ s\alpha s\beta c\gamma + c\alpha s\gamma & c\alpha c\gamma - s\alpha s\beta s\gamma & -s\alpha c\beta \\ s\alpha s\gamma - c\alpha s\beta c\gamma & c\alpha s\beta s\gamma + s\alpha c\gamma & c\alpha c\beta \end{bmatrix} \quad (2)$$

where β is the gondola pitch rotation angle, γ is the gondola yaw rotation angle, and α is the gondola roll rotation angle. Since the G-acceleration vectors in the BF and IF are known for time instant $i - 1$, the gondola rotation angles can be estimated for time instant i . The angular velocity and angular acceleration of gondola roll, pitch, and yaw axes ($\dot{\alpha}$, $\dot{\beta}$, $\dot{\gamma}$, $\ddot{\alpha}$, $\ddot{\beta}$, $\ddot{\gamma}$) can be determined through integration. Once the G-acceleration vector and gondola rotation angles are known in the IF, the remaining HCS kinematics and dynamics can be determined.

The HCS G-acceleration vector in the IF can be defined as

$$\mathbf{a} = [\mathcal{g}_X \quad \mathcal{g}_Y \quad \mathcal{g}_Z]^T \quad (3)$$

where \mathcal{g}_X is G-acceleration along the IF x-axis, \mathcal{g}_Y is G-acceleration along the IF y-axis, and \mathcal{g}_Z is G-acceleration along the IF z-axis. Since the HCS base has the same orientation as the IF and the HCS arm rotates around the base's z-axis, \mathbf{a} can be redefined as

$$\mathbf{a} = [a_t/g \quad a_c/g \quad 1]^T \quad (4)$$

where a_t , a_c , and g are the tangential acceleration, centripetal acceleration, and gravitational acceleration acting on the gondola. Tangential acceleration can be defined as

$$a_t = \dot{\omega}_{arm} \times r_{eff} \quad (5)$$

where $\dot{\omega}_{arm}$ is arm angular acceleration and r_{eff} is the effective radius of the end-effector from the CoR. The effective radius is defined as

$$r_{eff} = l_{arm} + (\mathbf{R}\mathbf{p}_{chest}) \quad (6)$$

where l_{arm} is the fixed arm length, \mathbf{R} is the rotational transformation matrix defined in equation (2), and \mathbf{p}_{chest} is the position vector of the user's chest CoM.

$$\mathbf{p}_{chest} = \mathbf{d}_{chest} + \mathbf{p}_s \quad (7)$$

where \mathbf{d}_{chest} is the displacement vector of the user's chest CoM from the position of the gondola seat and \mathbf{p}_s is the position vector of the gondola seat within the gondola. The seat position vector and all position vectors relating to the user's body within the gondola are expressed in the gondola BF.

Centripetal acceleration can be defined as

$$a_c = \omega_{arm} \times (\omega_{arm} \times r_{eff}) \quad (8)$$

where ω_{arm} is arm angular velocity.

Using Equations (3)–(5) and (8), arm angular velocity and arm angular acceleration can be redefined as

$$\omega_{arm} = \left((\mathcal{g}_Y g) / r_{eff} \right)^{1/2} \quad (9)$$

$$\dot{\omega}_{arm} = (\mathcal{g}_X g) / r_{eff} \quad (10)$$

2.2. Inverse Dynamic Analysis

HCS dynamic parameters useful to this study include shear force acting on the base, arm bending torque, and the maximum torques of the arm and gondola actuators. These parameters provide insight on the criteria for the HCS actuators and the structural integrity of the rotating structure, which in turn influence the cost of the HCS.

Shear force acting on the base can be defined as

$$f_{shear} = \omega_{arm}^2 \cdot [m_{gon}r_{eff} + m_{arm}l_{arm,CoM} - m_{cw}l_{cw,CoM}] \quad (11)$$

where f_{shear} is the shear force, m_{gon} is the gondola mass, m_{arm} is the arm mass, m_{cw} is the counterweight mass, and $l_{cw,CoM}$ is the distance from the counterweight CoM to the HCS CoR. Gondola mass can be defined as

$$m_{gon} = m_{gon\ structure} + m_u + m_e \quad (12)$$

where $m_{gon\ structure}$ is the mass of the gondola structure, m_u is the user mass, and m_e is the mass of the additional equipment in the gondola. Counterweight mass can be defined as

$$m_{cw} = m_{gon} + m_{arm} \quad (13)$$

The distance from the counterweight CoM to the HCS CoR can be defined as

$$l_{cw,CoM} = (m_{gon}r_{eff} + m_{arm}l_{arm,CoM}) / m_{cw} \quad (14)$$

Bending torque acting on the base can be defined as

$$\tau_{bend} = g \cdot [m_{gon}r_{eff} + m_{arm}l_{arm,CoM} - m_{cw}l_{cw,CoM}] \quad (15)$$

where τ_{bend} is the bending torque.

The arm actuator torque required to rotate the HCS structure around the base's vertical axis can be obtained as

$$\tau_{arm} = I_Z \dot{\omega}_{arm} \quad (16)$$

where τ_{arm} is the arm actuator torque and I_Z is the moment of inertia of the HCS rotating structure, which includes the arm, gondola, and counterweight. The moment of inertia can be defined as

$$I_Z = \sum m_i d_i^2 \quad (17)$$

where m_i is HCS rotating structure mass and d_i is the displacement of the rotating structure CoM relative to the CoR.

Gondola actuator torques required to rotate the gondola about the BF are defined as

$$\tau_{roll} = I_{gon,r} \ddot{\alpha} \quad (18)$$

$$\tau_{pitch} = I_{gon,p} \ddot{\beta} \quad (19)$$

$$\tau_{yaw} = I_{gon,y} \ddot{\gamma} \quad (20)$$

where τ_{roll} , τ_{pitch} , and τ_{yaw} are gondola roll, pitch, and yaw actuator torques, respectively, and $I_{gon,j}$ is the moment of inertia of the gondola around the respective axis j . The moment of inertia depends on the effective mass of the gondola user and equipment. The moment of inertia can be calculated as

$$I_{gon,j} = \sum m_{gon} d_{gon,j}^2 \quad (21)$$

where $d_{gon,j}$ is the displacement of the gondola CoM relative to the gondola's CoR.

3. Problem Formulation

3.1. Objective Functions

This section presents the objective functions of the multi-objective design optimisation and identifies the correlation between the optimisation objectives and HCS configurational design parameters. The HCS configurational design optimisation has three main objectives. The three primary objectives are the minimisation of Coriolis acceleration, FHAR, and cost. Gondola roll, pitch, and yaw rotation parameters will be analysed subject to the optimised configurational design parameters to determine the rotation requirements and reduce system complexity and cost.

(1) Coriolis acceleration at the head CoM of the HCS user.

Coriolis acceleration is calculated at the user's head and can be defined as

$$\mathbf{a}_{cor} = 2\boldsymbol{\omega}_{arm} \times \mathbf{v}_{rel,head} \quad (22)$$

where \mathbf{a}_{cor} is Coriolis acceleration vector at the user's head, $\boldsymbol{\omega}_{arm} = [0 \ 0 \ \omega_{arm}]^T$, and $\mathbf{v}_{rel,head}$ is the relative velocity vector of the user's head. The relative velocity of the user's head can be defined as

$$\mathbf{v}_{rel,head} = \left(\begin{bmatrix} \dot{\alpha} & \dot{\beta} & \dot{\gamma} \end{bmatrix}^T \times \mathbf{p}_{head} \right) + \mathbf{v}_{head} \quad (23)$$

where $\dot{\alpha}$ is roll angular velocity, $\dot{\beta}$ is pitch angular velocity, $\dot{\gamma}$ is yaw angular velocity, \mathbf{p}_{head} is the position vector of the user's head CoM, and \mathbf{v}_{head} is the velocity vector of the user's head. The position vector of the user's head CoM is calculated relative to the seat position vector and so is defined as

$$\mathbf{p}_{head} = \mathbf{d}_{head} + \mathbf{p}_s \quad (24)$$

where \mathbf{d}_{head} is the displacement vector of the user's head CoM from the gondola seat.

(2) Ratio of centripetal acceleration experienced at the feet and head of the HCS user FHAR can be defined as

$$\mathbf{a}_{FHAR} = a_{c,feet} / a_{c,head} \quad (25)$$

where $a_{c,feet}$ is centripetal acceleration at the user's feet and $a_{c,head}$ is centripetal acceleration at the user's head. Centripetal acceleration at the user's feet can be defined as

$$a_{c,feet} = \boldsymbol{\omega}_{arm} \times \left(\boldsymbol{\omega}_{arm} \times [0 \ -r_{feet} \ 0]^T \right) \quad (26)$$

where r_{feet} is the effective radius of the user's feet from the CoR. r_{feet} is obtained as

$$r_{feet} = l_{arm} - \mathbf{R}\mathbf{p}_{feet} \quad (27)$$

where \mathbf{p}_{feet} is the position vector of the user's feet CoM and defined as

$$\mathbf{p}_{feet} = \mathbf{d}_{feet} + \mathbf{p}_s \quad (28)$$

where \mathbf{d}_{feet} is the displacement vector of the user's feet CoM from the gondola seat.

Centripetal acceleration at the user's head can be defined as

$$a_{c,head} = \boldsymbol{\omega}_{arm} \times \left(\boldsymbol{\omega}_{arm} \times [0 \ -r_{head} \ 0]^T \right) \quad (29)$$

where r_{head} is the effective radius of the user's head from the CoR. r_{head} is calculated as

$$r_{head} = l_{arm} - (\mathbf{R}\mathbf{p}_{head}) \quad (30)$$

(3) Cost of the HCS

A main limiter of HCS design and motion capability is budget and, thus, cost. Cost has a twofold purpose as an optimisation objective. Firstly, cost sets a standard objective to reduce manufacturing costs and the overall cost of a product whilst still achieving the desired product quality and capability. Secondly, cost serves as the primary reason for deeming a shorter arm length as more desirable than a longer arm length. Without cost as an objective, the longest feasible arm length can be considered as the optimal arm length to reduce Coriolis and FHAR; however, this creates issues of large inertia and contributes to the issue of HCSs motion response delay.

Cost is linked to the type of structure, amount of material, and type of actuators required to develop and operate the HCS. Cost can also be linked to the size of the HCS, as it affects the space and cost of the infrastructure required to house the system. HCS design and development costs can be defined as the summation of the costs of the HCS base, arm, counterweight, gondola, and respective actuators. This study considers electric motors for arm and gondola actuation. Thus, HCS costs can be represented by a cost index consisting of mass and induced forces due to the facts that (1) material cost increases with quantity and structural strength, and (2) mass influences the requirement for a motor with greater torque capability. For this reason, costs are indirectly calculated using HCS mass-affecting material costs in addition to HCS inertia. Since cost is indirectly calculated, it is represented by a cost index throughout this study. The cost index can be defined as

$$c_{HCS} = c_b + c_{arm} + c_{arm,m} + c_{cw} + c_{gon} + c_{gon,m} \quad (31)$$

where c_{HCS} is the HCS, c_b is the base, c_{arm} is the arm, $c_{arm,m}$ is the arm motor, c_{cw} is the counterweight, c_{gon} is the gondola, and $c_{gon,m}$ is the gondola motor cost indices. The cost index of the HCS base can be indirectly defined as

$$c_b = k_b(f_{shear} + \tau_{bend}) \quad (32)$$

where k_b is the cost coefficient for the base. The cost index of the HCS arm is assumed as

$$c_{arm} = k_{arm}l_{arm} \quad (33)$$

where k_{arm} is the cost coefficient for the arm. The cost index of the HCS arm motor is proposed as

$$c_{arm,m} = k_{arm,m}\tau_{arm} \quad (34)$$

where $k_{arm,m}$ is the cost coefficient for the arm motor. The cost index of the HCS counterweight is assumed as

$$c_{cw} = k_{cw}m_{cw}l_{cw} \quad (35)$$

where k_{cw} is the cost coefficient for the counterweight and l_{cw} is the mounting radius of the counterweight. The cost index of the HCS gondola can be indirectly defined as

$$c_{gon} = k_{gon}l_{gon}w_{gon}h_{gon} \quad (36)$$

where k_{gon} is the cost coefficient for the gondola, l_{gon} is the gondola length, w_{gon} is the gondola width, and h_{gon} is the gondola height. The cost index of the gondola motors can be indirectly defined as

$$c_{gon,m} = k_{gon,m}(\tau_{roll} + \tau_{pitch} + \tau_{yaw}) \quad (37)$$

where $k_{gon,m}$ is the cost coefficient for the gondola motor.

Based on Equations (8), (9), and (22)–(30), vestibular Coriolis and FHAR are directly affected by arm length and seat position. Cost is directly affected by mass and structural strength, which are directly proportional to arm length and the size of the gondola required to accommodate the desired seat position. Therefore, the design parameters are arm length

and seat position. The required RoM of the gondola motors will also be obtained, as they are critical values for the identification of the required motor properties in addition to the motor torques.

3.2. Design Parameters and Constraints

Arm length and seat position are the two key HCS configurational design parameters. All objectives are affected by arm length and seat position and can be minimised or maximised based on these parameters. The design parameter vector can be defined as

$$\mathbf{x} = [l_{arm}, p_{s, x}, p_{s, y}, p_{s, z}] \quad (38)$$

where $p_{s, x}$, $p_{s, y}$, and $p_{s, z}$ are the x, y, and z components of the gondola seat position vector. Arm length was given the lower and upper constraints of 5 m and 18 m based on the lengths of current systems. This limits arm length optimisation to known feasible parameters. Seat position with respect to the gondola CoR was given the lower and upper constraints of ± 0.5 m along the x and y axes and -1.25 m and -0.25 m along the z-axis. The seat position constraints limit the user's head to be within ± 0.5 m from the gondola CoR. If the seat position distance is increased beyond the selected constraints, it is deemed that the gondola will become too large. After reviewing the optimisation results, broadening the seat position constraints was deemed unnecessary.

HCS DoF and gondola RoM are optimised with respect to the error between HCS and aircraft G-acceleration vectors. DoF can be optimised manually through trial and error. Based on the research provided in [9], this study investigates the optimisation of a four-DoF HCS. RoM can be optimised by analysing the minimum and maximum rotation angles required to replicate the aircraft G-acceleration vectors. These rotation angles are determined with an optimisation solver during the IKD analysis.

3.3. Formulation of the Optimisation Problem

The optimisation process consists of a global multi-objective optimiser minimising several cost criteria subject to the configurational design constraints using the presented mathematical model of an active four-DoF HCS. Based on the presented objective functions, design parameters, and constraints, the multi-objective optimisation solver will solve for the HCS arm length and seat position that minimise Coriolis and system cost and minimise the deviation of FHAR from 1. The model of the configurational design optimisation problem can be formulated as

$$\text{Minimise } J = [a_{cor}^2, (a_{FHAR} - 1)^2, c_{HCS}^2] \quad (39)$$

subject to:

$$x_{lb} \leq \mathbf{x} \leq x_{ub}$$

where J is the set of objective functions to be minimised and \mathbf{x} is the design parameter vector bound by upper and lower bounds (x_{ub} , x_{lb}).

4. Configurational Design Optimisation Method

The desired HCS output at the end-effector consists of three G-acceleration profiles obtained from three ACMs. The ACMs consist of the Barrel Roll, Loop, and High Yo-Yo combat manoeuvres (Figure 4). These ACMs are discussed in detail in [53,54], and simulation of these ACMs and analysis of the resulting G-acceleration vectors are presented and discussed in [9]. Each ACM has a 30 s duration, and the aircraft maintains a forward velocity of 200 m/s throughout. The Barrel Roll and High Yo-Yo ACMs consist of roll and pitch rotation and incur between -1 G and 1 G along the x- and y-axes of the aircraft end-effector (CoM of the pilot's chest) and generate 7 G and 6.5 G, respectively, along the z-axis of the end-effector. The Loop ACM performs a pure pitch loop and so does not generate G-acceleration along the y-axis but incurs -1 G to 1 G along the x-axis from

gravitational acceleration and generates 10 G along the z-axis of the end-effector. The optimisation is performed with four trials corresponding to four ACMs. Trial 1, Trial 2, and Trial 3 use the Barrel Roll, Loop, and High Yo-Yo manoeuvre, respectively, as the motion input. The fourth optimisation trial simulates the three ACMs consecutively as one long manoeuvre to counteract optimising the HCS configurational design for one specific ACM. The optimisation scenarios are presented in Table 1.

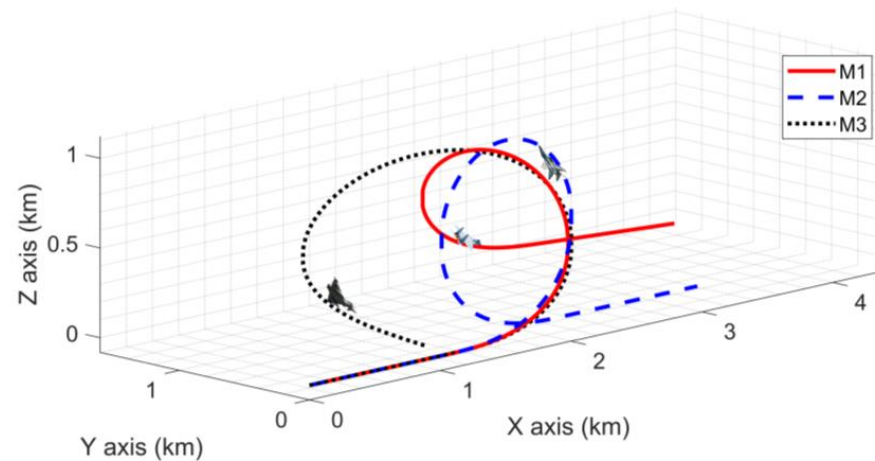


Figure 4. Trajectories of the Barrel Roll (M1), Loop (M2), and High Yo-Yo (M3) Aircraft Combat Manoeuvres.

Table 1. Optimisation scenarios.

Optimisation Trial	Aircraft Manoeuvre	Objectives
1	Barrel Roll	Coriolis/FHAR/ Cost Index
2	Loop	
3	High Yo-Yo	
4	All combined	

Optimisation is performed with a controlled, elitist Genetic Algorithm (GA) using MATLAB's *gamultiobj* solver, which is a variant of NSGA-II. This function was selected as it is the primary global multi-objective optimisation solver offered with MATLAB, which uses a robust optimisation technique to perform a global search in the solution space for the global optimum point [55,56]. GA multi-objective optimisations and their use in parametric optimisation have been widely researched and are discussed within the literature such as [57–60]. Additionally, the limitations of mathematical models are discussed in [61]. The optimisation method is presented in Figure 5. With respect to the optimisation trial, the *gamultiobj* solves for the arm length and seat position that best minimise the Coriolis, FHAR, and cost index values produced via HCS motion required to replicate the respective ACM. Roll, pitch, and yaw RoM are obtained by observing the minimum and maximum angles required to replicate the inputted ACMs using the optimised configurational design parameters.

The operational kinematic inputs of the HCS are derived from the reference G-acceleration vectors using the presented HCS inverse kinematics method and the simulation method presented in [9]. Gondola roll, pitch, and yaw rotation are obtained by determining the matrix that transforms the achieved IF G-acceleration vector of the HCS into the reference G-acceleration vector defined in the end-effector BF. The gondola roll, pitch, and yaw angles are then extracted from the obtained transformation matrix. The angular velocity and acceleration of the HCS arm are obtained using the MATLAB optimisation solver function *fmincon*, which solves for the optimal arm rotation values that minimise the tracking error between the achieved and reference G-acceleration vectors. The solver uses the sequential

quadratic programming optimisation algorithm. The solver parameters are presented in Table 2.

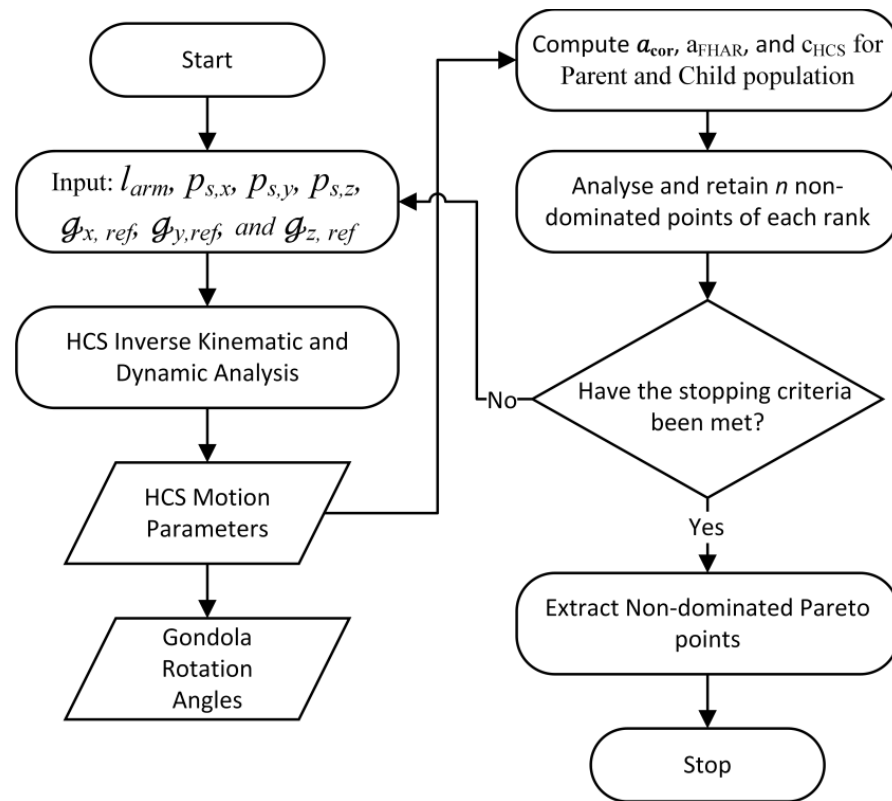


Figure 5. Implementation of gamultiobj.

Table 2. fmincon optimisation solver parameters.

fmincon Parameters	Value
Maximum Iterations	100
Optimality Tolerance	0.001
Step Tolerance	0.05
Function Tolerance	0.05
Constraint Tolerance	0.001

When reducing undesirable effects, other artefacts may appear and compromise the HCS’s capability to accurately replicate the desired G-acceleration vectors. Thus, it is important to investigate whether the optimum configurational design solutions detrimentally impact the HCS performance of the desired G-acceleration vectors. The accurate replication of the reference G-acceleration vectors is not evaluated during the multi-objective optimisation of the HCS configurational design parameters. The HCS performance of the ACMs will be investigated through analysis of the resulting tracking errors for each of the optimal configurational design solutions.

4.1. Optimisation Solver Parameters

The optimisation solver parameters were set to their best values through trial and error and observation of the parameters of other research. The best values were determined through the optimisation solver’s ability to produce the best solutions. The best solutions are those with the largest spread of points and minimisation of the objectives simultaneously. This is a common method used to determine optimisation solver parameters [39,56,62]. The key solver parameters are presented in Table 3. The stopping criteria of gamultiobj are when the geometric average change in the spread of Pareto solutions is less than the

function tolerance and the final spread is less than the mean spread over the previous maximum number of stall generations. The resulting number of solutions in the Pareto front is dependent on the solver's performance. Solutions are selected based on their ability to minimise all cost criteria and each individual criterion.

Table 3. MATLAB multi-objective optimiser parameters.

Optimisation Parameters	Values
Population Size	100
Crossover Fraction	0.8
Migration Fraction	0.2
Pareto Fraction	0.35
Generations Limit	100
Stall Generations Limit	50
Function Tolerance	1×10^{-4}
Estimated Computation Time	6 h

4.2. Human Centrifuge System Parameters

The displacement vectors of the user's head, feet, and chest CoMs from the SRF are presented in Table 4. These values are derived from the minimum aircrew anthropometrics for USAF fighter aircraft [63]. The vestibular system's vertical displacement from the gondola seat position is very similar to the user's sitting eye height. Thus, the mean minimum sitting eye height for USAF fighter aircraft was used to set the head displacement vector. In this work, seat reclination is not factored into head displacement relative to the SRF. The user's foot position is based on USAF aircrew buttock to knee length and sitting knee height [63]. The feet are assumed to be located slightly further from the buttock along the SRF x-axis than the knees, as aircrew legs are generally a few degrees from perpendicular to the aircraft floor.

Table 4. Displacement of human body parts from the seat body frame.

Body Part	Displacement from Seat Body Frame (m)		
	x-Axis	y-Axis	z-Axis
Head	0	0	0.75
Feet	0.65	0	−0.54
Chest	0	0	0.45

5. Optimisation Results

Using the presented optimisation method, optimal configurational design parameters that minimise Coriolis, FHAR, and system cost can be obtained. The resulting configurational design and corresponding Coriolis, FHAR, and cost index values are presented in this section. Additionally, the gondola rotational parameters for each of the optimal design parameters are presented. The resulting configurational design solutions for Optimisation Trials 1–4 are presented in Figure 6, Figure 7, Figure 8 and Figure 9, respectively. The Pareto optimal front for the minimisation of Coriolis, FHAR, and cost index with respect to arm length is presented in Figures 6a, 7a, 8a and 9a. The frequency of optimal seat position values is presented in a histogram with a distribution fit. Cost indices are scaled with respect to Coriolis and FHAR.

During HCS simulation of the Barrel Roll ACM, the arm length solution pool minimising Coriolis, FHAR, and cost is predominantly situated between 5 and 6 m (Figure 6a). However, this solution pool does not fully minimise Coriolis and FHAR. From 7 m, arm length stops having a significant effect on minimising Coriolis and FHAR. Arm length has a linear and direct effect on cost. As shown in Figure 6b, the seat position solution pool is predominantly situated between 0 and 0.5 m along the x-axis, between −0.45 and −0.1 m along the y-axis, and between −1 and −0.75 m along the z-axis.

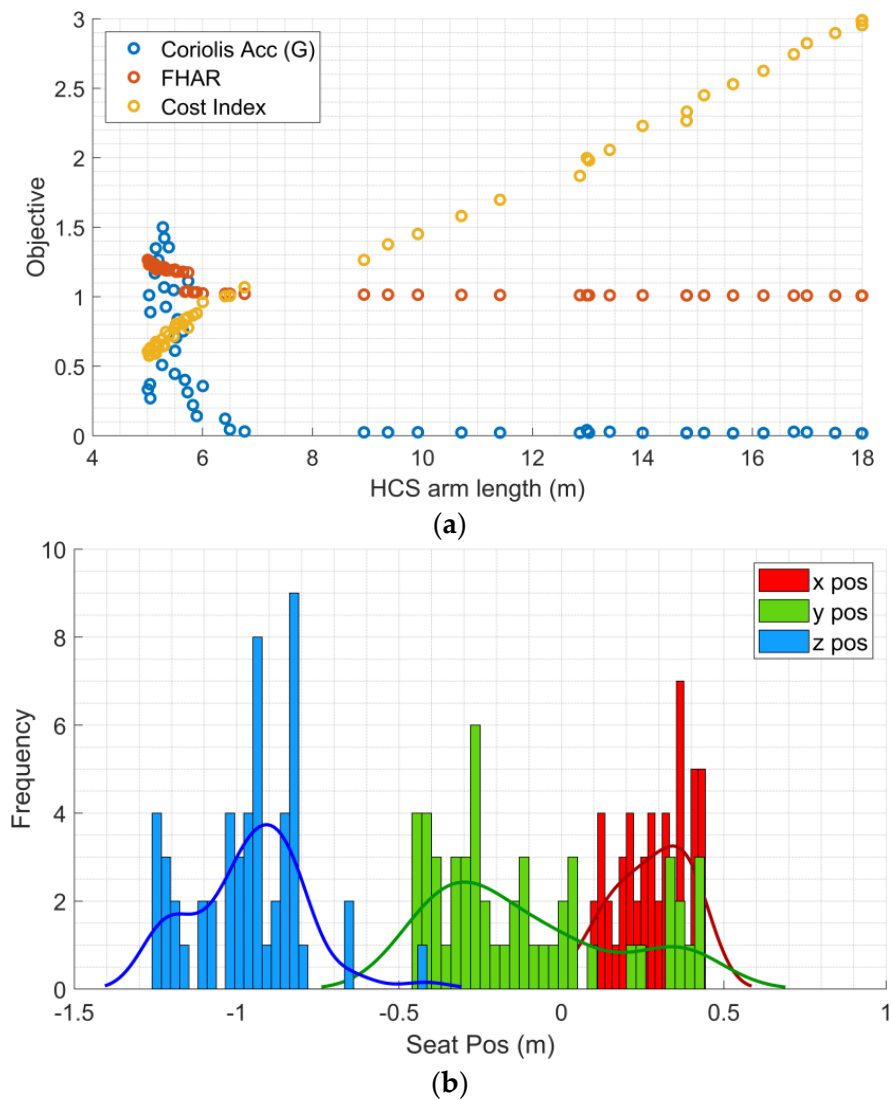


Figure 6. Multi-objective optimisation for the Barrel Roll manoeuvre. (a) The effect of arm length on Coriolis, FHAR, and cost index. (b) The distribution of optimal solutions for seat x, y, and z positions.

In Figure 7a, the arm length solution pool to minimise Coriolis, FHAR, and cost during HCS simulation of the Loop ACM is predominantly situated between 5 and 8 m, with no solutions for arm lengths of 10 to 14 m. Similarly, from 7 m, the effect of arm length on Coriolis and FHAR reduces significantly but remains consistent for cost. In Figure 7b, the seat position solution pool is predominantly situated between 0.35 and 0.5 m along the x-axis, between -0.1 and 0.15 m along the y-axis, and between -1.25 and -1 m along the z-axis.

In Figure 8a, the arm length solution pool to minimise Coriolis, FHAR, and cost during HCS simulation of the High Yo-Yo ACM is predominantly situated between 5 and 6 m. These solutions, however, do not fully minimise Coriolis and FHAR. From 6 m, the effect of arm length on FHAR reduces significantly. However, 6.5 m greatly minimises Coriolis, but from 7 m, Coriolis increases and gradually decreases several times before reaching the global minima at approximately 16 m. Akin to the previous two optimisation trials, the increase in arm length has a consistent linear and direct effect on cost. In Figure 8b, the seat position solution pool is predominantly situated between 0.3 and 0.6 m along the x-axis, between -0.35 and 0 m along the y-axis, and between -1.2 and -0.7 m along the z-axis.

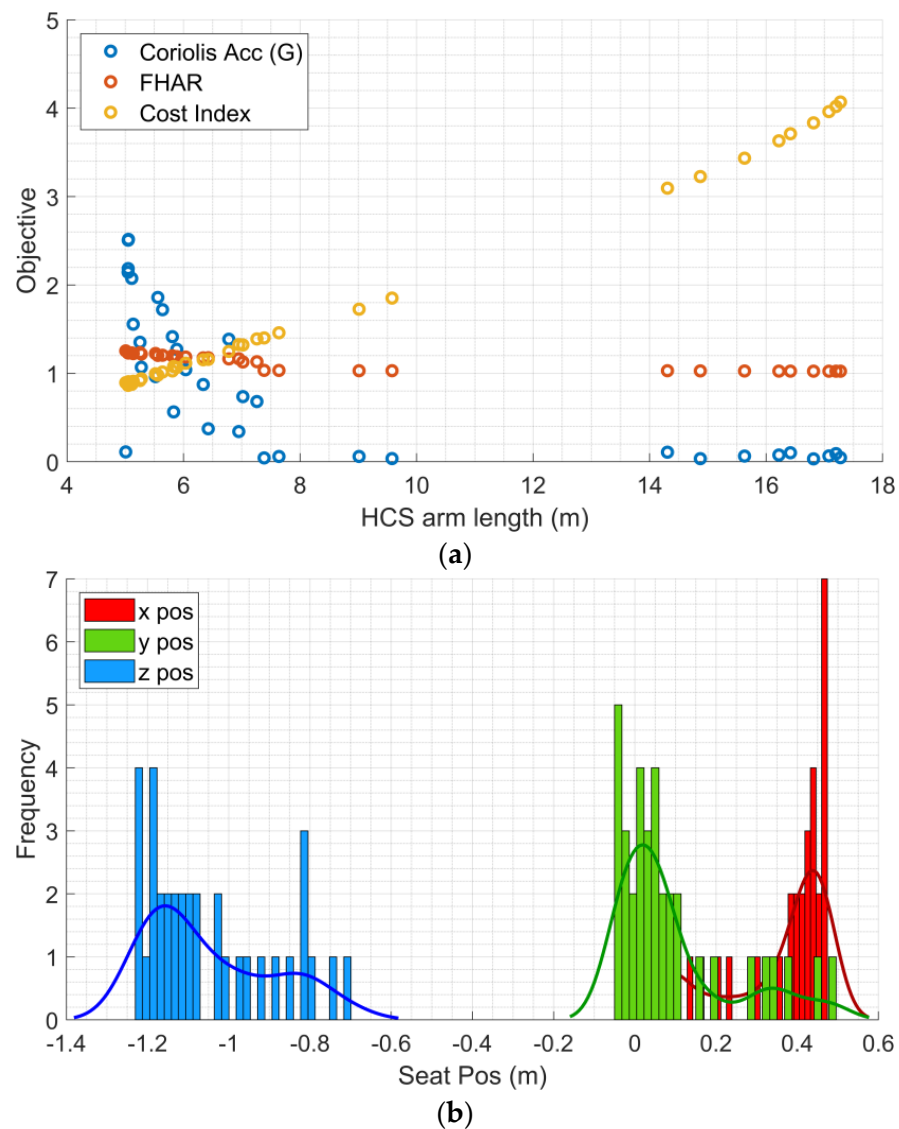


Figure 7. Multi-objective optimisation for the Loop manoeuvre. (a) The effect of arm length on Coriolis, FHAR, and cost index. (b) The distribution of optimal solutions for seat x, y, and z positions.

Figure 9 presents the multi-objective optimisation results from Trial 4, which sought the minimisation of the HCS cost index and the Coriolis and FHAR produced during HCS simulation of all three ACMs. In Figure 9a, the arm length solution pool to minimise Coriolis, FHAR, and cost during HCS simulation of all three ACMs is predominantly situated between 6 and 9 m, with the global minimum of each of the objectives occurring within this solution space. No solutions are observed for arm lengths of 9 to 17 m. In Figure 9b, the seat position solution pool is predominantly situated between 0 and 0.3 m along the x-axis, between -0.3 and -0.1 m along the y-axis, and between -1 and -0.8 m along the z-axis.

The global optimum Coriolis, FHAR, and cost index values and the corresponding design parameter values for each of the four optimisation trials are presented in Tables 5–8. Table 8 presents the best design parameter values for the minimisation of each objective during the HCS simulation of all three ACMs. For optimisation trials 1, 2, and 3, the optimum arm length values minimising the maximum experienced Coriolis and FHAR are between 16 m and 18 m, which is twice the length of the average HCS arm, and the optimum arm length value to minimise cost is approximately 5 m. These results were expected based on Equations (22), (25) and (31). However, for optimisation Trial 4, the optimum arm length minimising Coriolis and FHAR is between 8 m and 9 m, which is

significantly shorter than the optimum values for the preceding trials and is approximately the standard arm length of current HCS. Additionally, the optimal arm length to minimise cost is 6 m.

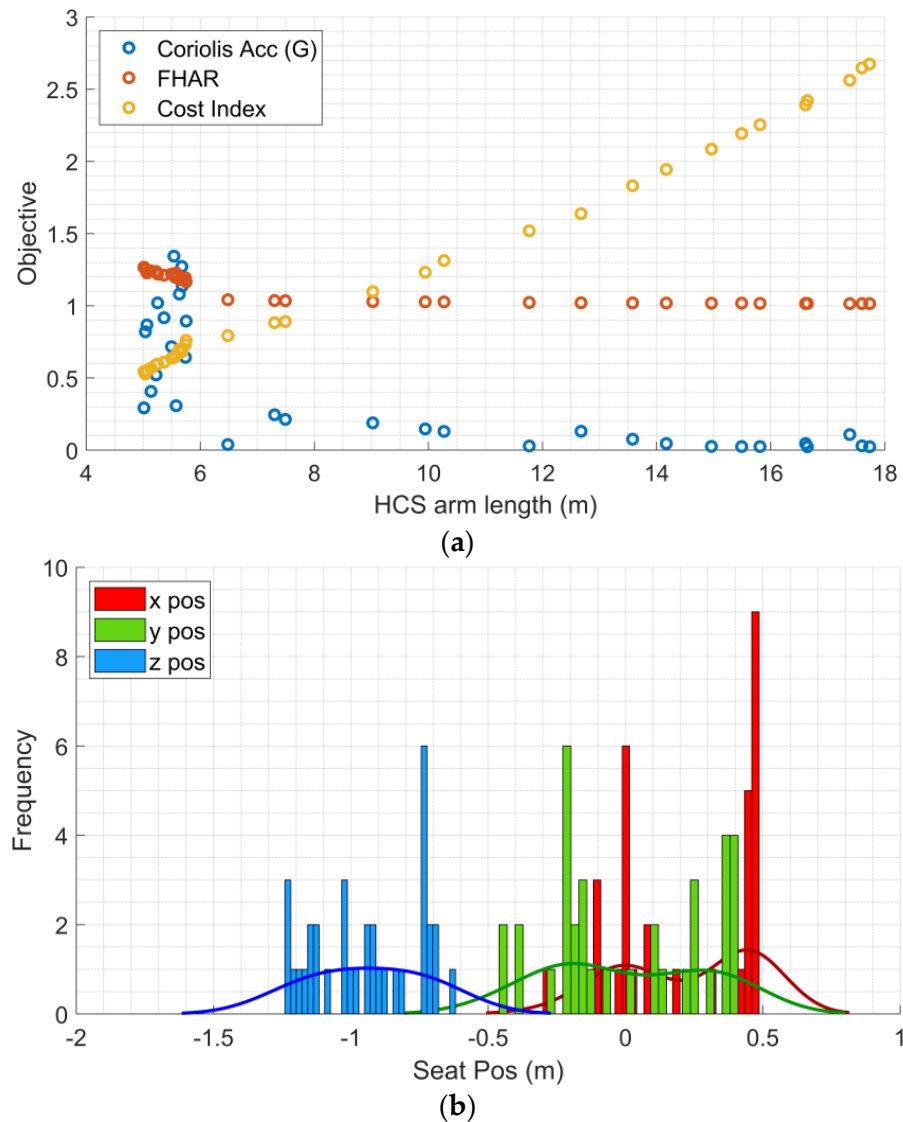


Figure 8. Multi-objective optimisation for the High Yo-Yo manoeuvre. (a) The effect of arm length on Coriolis, FHAR, and cost index. (b) The distribution of optimal solutions for seat x, y, and z positions.

Table 5. Optimal design parameters for replication of the Barrel Roll manoeuvre.

Objective	Optimal Value	Corresponding Design Parameters			
		Arm Length (m)	Seat Position (m)		
			x	y	z
Coriolis Acc (G)	0.017	17.997	0.112	−0.452	−0.832
FHAR	1.008	17.988	0.145	−0.444	−0.824
Cost Index	0.576	5.028	0.367	0.425	−1.242

The optimal seat position values along the x-axis to minimise Coriolis are between −0.019 m and 0.112 m, with Trial 4 resulting in a value of 0.020 m. To minimise FHAR, the optimal seat position values along the x-axis are between 0.110 m and 0.470 m, with 0.110 m being the optimum solution for Trial 4. The optimal seat position values along the y-axis to minimise Coriolis are between −0.452 m and 0.047 m, with Trial 4 resulting

in a value of -0.170 m. To minimise FHAR, the optimal seat position values along the y-axis broadly ranged between -0.444 m and 0.443 m, with -0.088 m being the optimum solution for Optimisation Trial 4. The optimal seat position values along the z-axis to minimise Coriolis are between -0.832 m and -0.713 m, with optimisation Trial 4 resulting in a value of -0.803 m. To minimise FHAR, the optimal seat position values along the z-axis are between -1.072 m and -0.621 m, with -0.946 m being the optimum solution for optimisation Trial 4. Seat position has no effect on HCS cost other than to provide criteria for the gondola size required to accommodate the seat position. Thus, the seat position values provided for the cost index global optimum are to best minimise Coriolis and FHAR at the given arm length and cost index.

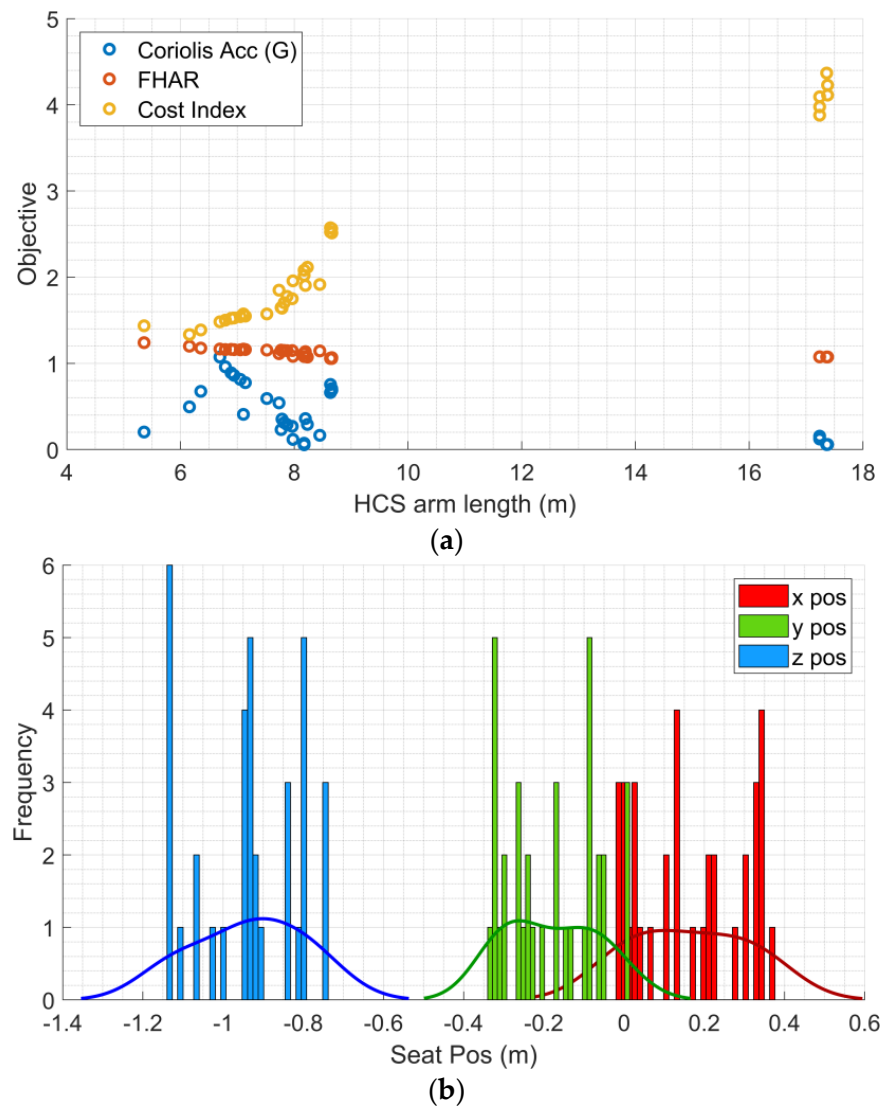


Figure 9. Multi-objective optimisation for all three manoeuvres. (a) The effect of arm length on Coriolis, FHAR, and cost index. (b) The distribution of optimal solutions for seat x, y, and z positions.

To analyse whether changing the configurational design parameters has a detrimental impact on the HCS performance of ACMs, the tracking errors between the achieved and reference G-acceleration vectors are investigated. Table 9 presents the maximum and Root Mean Square (RMS) tracking errors for the four-DoF HCS using the optimal configurational design parameter solutions for each minimised objective value. According to the maximum tracking errors, a short arm length detrimentally impacts the HCS performance of the three

ACMs. However, the RMS tracking error is still small, regardless of the arm length and seat position. The largest RMS tracking error is 0.125 G along the z-axis of the HCS end-effector.

Table 6. Optimal design parameters for the replication of the Loop manoeuvre.

Objective	Optimal Value	Corresponding Design Parameters			
		Arm Length (m)	Seat Position (m)		
			x	y	z
Coriolis Acc (G)	0.033	16.815	0.079	0.047	−0.821
FHAR	1.025	17.200	0.470	0.443	−1.072
Cost Index	0.864	5.049	0.468	−0.050	−1.213

Table 7. Optimal design parameters for the replication of High Yo-Yo manoeuvre.

Objective	Optimal Value	Corresponding Design Parameters			
		Arm Length (m)	Seat Position (m)		
			x	y	z
Coriolis Acc (G)	0.024	16.643	−0.019	−0.228	−0.713
FHAR	1.015	17.598	0.464	−0.155	−0.621
Cost Index	0.517	5.039	−0.115	0.407	−1.012

Table 8. Optimal design parameters for the replication of all three manoeuvres.

Objective	Optimal Value	Corresponding Design Parameters			
		Arm Length (m)	Seat Position (m)		
			x	y	z
Coriolis Acc (G)	0.055	8.174	0.020	−0.170	−0.803
FHAR	1.056	8.637	0.110	−0.088	−0.946
Cost Index	1.334	6.157	0.224	−0.244	−0.930

Table 9. Maximum and RMS tracking error for HCS replication of all three ACMs.

Trial	Minimised Objective	Arm Length (m)	Seat Position (m)	Max Error (G)	RMS Error (G)
			[x, y, z]	[Gx, Gy, Gz]	[Gx, Gy, Gz]
1	Coriolis Acc	17.997	[0.112, −0.452, −0.832]	[0.045, 0.038, 0.183]	[0.013, 0.010, 0.025]
	FHAR	17.988	[0.145, −0.444, −0.824]	[0.044, 0.038, 0.282]	[0.012, 0.010, 0.025]
	Cost Index	5.028	[0.367, 0.425, −1.242]	[0.311, 0.966, 0.899]	[0.053, 0.046, 0.094]
2	Coriolis Acc	16.815	[0.079, 0.047, −0.821]	[0.041, 0.025, 0.201]	[0.014, 0.008, 0.026]
	FHAR	17.200	[0.470, 0.443, −1.072]	[0.097, 0.044, 0.269]	[0.016, 0.011, 0.025]
	Cost Index	5.049	[0.468, −0.050, −1.213]	[0.549, 1.763, 2.286]	[0.047, 0.047, 0.124]
3	Coriolis Acc	16.643	[−0.019, −0.228, −0.713]	[0.027, 0.035, 0.190]	[0.013, 0.010, 0.026]
	FHAR	17.598	[0.464, −0.155, −0.621]	[0.029, 0.032, 0.189]	[0.012, 0.010, 0.026]
	Cost Index	5.039	[−0.115, 0.407, −1.012]	[0.625, 1.094, 1.428]	[0.055, 0.046, 0.125]
4	Coriolis Acc	8.174	[0.020, −0.170, −0.803]	[0.048, 0.032, 0.262]	[0.019, 0.012, 0.036]
	FHAR	8.637	[0.110, −0.088, −0.946]	[0.086, 0.025, 0.214]	[0.020, 0.011, 0.035]
	Cost Index	6.157	[0.224, −0.244, −0.930]	[0.180, 0.608, 0.911]	[0.029, 0.026, 0.046]

The improvement of Coriolis acceleration and FHAR throughout the performance of all three ACMs compared to those obtained using general design values of a four-DoF HCS are presented in Figure 10 and Table 10. The general design values are taken from the four-DoF HCS presented in [9]. The arm length and position of the end-effector in the HCS for the general-design HCS are presented in Table 11. Table 10 presents the RMS errors of Coriolis and FHAR at 0 and 1, respectively. The results show that the optimal design parameters not only minimise Coriolis and FHAR experienced during the ACMs but also smooth out peaks in Coriolis caused by the motion of the gondola to redirect centripetal acceleration according to the ACM motion profiles.

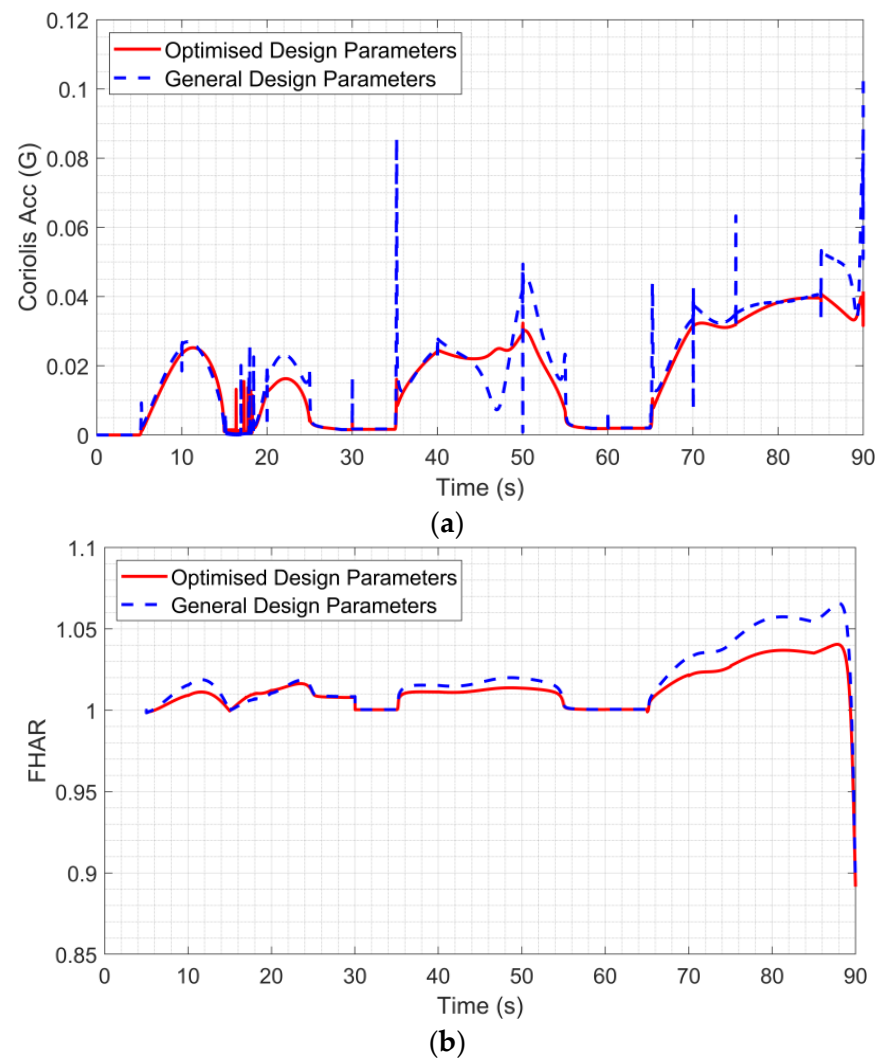


Figure 10. Comparison of the optimum and generally selected configurational design parameters, (a) comparison of the Coriolis acceleration, and (b) comparison of the FHAR.

Table 10. Comparison of objective values for the optimum and generally selected configurational design parameters.

Objective	Optimal Design RMS Error	General Design RMS Error
Coriolis (G)	0.0216	0.0245
FHAR	0.0185	0.0273

Table 11. General design values for a four-axis Human Centrifuge System.

HCS Parameter	Value
HCS arm length (m)	5
Seat offset from the gondola CoR (m) [x, y, z]	[-0.5, 0, -0.80]
Displacement of user's chest CoM from the seat BF (m) [x, y, z]	[0, 0, 0.45]

Table 12 presents the gondola rotational parameters from Trial 4 that correspond to the optimal configurational design values of each minimised objective criteria produced during the HCS simulation of all three ACMs. The required RoM and maximum RPM of roll, pitch, and yaw rotation are essentially identical for the minimised objectives of Coriolis

and FHAR. From the results, it can be observed that the gondola requires roll rotation ranging from -90 to 50 degrees, pitch rotation ranging from -2 to 87 degrees, and yaw rotation ranging from -30 to 86 degrees. Cost index minimisation results in greater RPM requirements than the minimisation of Coriolis and FHAR. This can be attributed to the shortening of the HCS arm length for the minimisation of the cost index, which results in the need for higher RPM speeds and a greater change in gondola orientation per time instant to generate the desired G-acceleration motion profiles.

Table 12. Roll, pitch, and yaw parameters required for the HCS simulation of ACMs.

Gondola Rotation	Minimised Objective	Rotation Parameters			
		Min (deg)	Max (deg)	RoM (deg)	Max RPM
Roll	Coriolis	-89.7	49.5	139.2	48.8
	FHAR	-89.7	49.5	139.2	48.8
	Cost Index	-86.5	48.2	134.7	48.5
Pitch	Coriolis	0	86.7	86.7	70.4
	FHAR	0	86.7	86.7	70
	Cost Index	-1.4	78.5	79.8	205.5
Yaw	Coriolis	-28.2	85.5	113.6	44.6
	FHAR	-28.3	85.6	113.8	45.4
	Cost Index	-17.1	78.1	95.2	70

6. Discussion

From the results of the multi-objective optimisation of HCS configurational design, it can be observed that the performance of a HCS can be improved using a four-DoF HCS with an arm length of approximately 8 m and the end-effector located forward left and slightly lower than the gondola CoR. Arm length has an inverse relationship with Coriolis and FHAR and has a direct relationship with the cost of the HCS system. For arm lengths between 5 m and 9 m, the inverse relationship with Coriolis is profound but greatly reduced for arm lengths longer than 8 m. Arm length has significantly less effect on the minimisation of FHAR, but it also primarily reduces FHAR between the lengths of 5 and 9 m, with little effect beyond these lengths. Arm length has a direct and almost linear effect on the cost index. Therefore, extending the arm length beyond 9 m will have a greater increase in cost than a beneficial decrease in Coriolis and FHAR. Since cost is a critical factor, the optimal solution is dependent on the discretion of the HCS budget.

The user's head should have positive x and negative y and z positions with respect to the gondola CoR. Seat position and orientation affect the motion field experienced by users during gondola roll, pitch, and yaw rotation. Increasing seat x position causes a decrease in the user's effective distance from the arm CoR during positive gondola yaw rotation and an increase during negative gondola yaw rotation. These are the opposites for decreasing the seat x position. Increasing seat y position causes a decrease in the user's effective distance from the arm CoR during gondola roll and yaw rotation. Opposite results have been observed for decreasing the seat y position. Increasing seat z position causes a decrease in the user's effective distance from the arm CoR during positive gondola roll rotation and an increase during negative gondola roll rotation. Opposite changes have been observed for decreasing the seat z position. An increase or decrease in the user's effective distance from the arm CoR affects the resulting magnitude of centripetal acceleration on the user.

Optimising the configurational design of a four-DoF HCS to minimise Coriolis and FHAR additionally reduced the tracking error of the system. The four-DoF HCS presented in [9] produced an RMS tracking error of 0.07 G and maximum tracking errors of 0.80 Gz, 0.59 Gz, and 0.62 Gz for the Barrel Roll, Loop, and High Yo-Yo ACMs, respectively. Using the arm length and seat position from Trial 4, the RMS tracking error did not exceed 0.047 G, and the maximum tracking errors did not exceed 0.086 G. The maximum errors occur for less than 0.3 s. The errors are caused by limitations in the estimation technique

and optimisation solver for calculating the operational kinematics of the HCS. Due to the cause of the errors, they can be potentially mitigated through the implementation of a suitable control technique.

Due to the nature of multi-objective optimisation and the limitations of mathematical models, the results of this study may not be a guaranteed global optimal solution. Rather, the results provide insight and a guide to the configurational design parameters of note and their overall effect on HCS performance. It is for each individual to discern the requirements and monetary limits of their HCS design and performance and then pursue the respective configurational design optimisation. Additionally, multi-objective optimisation does not minimise each objective criterion to the fullest possible extent. For example, Coriolis acceleration can be further minimised to the detriment of the other objectives by having the maximum possible arm length and positioning the seat to centre the user's head at the intersection of the gondola rotation axes, so that the user's head only changes orientation rather than location during gondola rotation. Thus, a compromise in the minimisation of each objective has been considered. Greater weight could be placed on the minimisation of Coriolis acceleration since FHAR can also be reduced using a G-suit and cost can be reduced through efficient material selection and structural design, which are not factored in this study's calculation of FHAR and cost.

7. Future Developments

Seat reclination was not incorporated into this study and therefore did not influence the head and chest positions. While training aircraft do use a 90 deg backrest angle, the majority of combat aircraft have a 13 deg to 30 deg backrest angle. This reduces the vertical head–heart distance of the aircrew. Seat reclination also reduces the vertical head-to-foot distance, which could potentially decrease the magnitude of FHAR. Future works should incorporate seat reclination in the multi-objective optimisation of HCS configurational design and investigate the impact of differing seat backrest angles on Coriolis and FHAR.

The torques and overall cost of the HCS were calculated with simplicity and focused on the influence of HCS arm length and seat position. Hence, a cost index was used to visualise how the change in HCS configurational design could affect the system cost. A detailed calculation of the torques and cost of each HCS component should be investigated in future works to provide a complete and comprehensive guide on how changes in configurational design fully impact the system cost.

In addition to seat position and arm length, another configurational design parameter investigated within this study was the addition of gondola yaw rotation. A four-DoF HCS seems more capable of replicating multi-axis G-acceleration profiles. However, it has yet to be determined whether a four-DoF HCS is more optimal than a three-DoF system. Future work should compare the performance capabilities of a four-DoF HCS and a three-DoF HCS and investigate the optimal DoFs for a HCS to replicate aircraft acceleration profiles.

This study provides a versatile framework to optimise HCS configurational design. While optimising configurational design does improve HCS performance, solely optimising HCS configurational design does not provide a complete solution to the overall optimisation of HCS performance. Using the optimal configurational design as the base model, further investigation is required on the optimisation of the operational parameters and motion control of the HCS to mitigate the tracking error. Additionally, the actuation requirements for the arm and gondola in an optimal configurational design are yet to be verified.

8. Conclusions

Human Centrifuge Systems (HCSs) are valuable motion systems for replicating multi-axis G-accelerations akin to aircraft and spacecraft. This study provides a framework to establish the relationship between the configurational design and performance of a four Degree-of-Freedom (DoF) HCS. The most important configurational design parameters and their relationship with HCS performance were determined using an Inverse Kinematic and Dynamic (IKD) analysis. Moreover, global multi-objective optimisation was proposed

to find the optimal configurational design parameters using three different Aircraft Combat Manoeuvres (ACMs) as the HCS reference motion. The configurational design parameters consist of arm length and seat position, and the optimisation objective criteria consist of Coriolis acceleration, Feet-to-Head Acceleration Ratio (FHAR), and implementation cost.

The multi-objective optimisation results show that optimisation of the configurational design of a HCS improves the performance of the system through minimisation of undesired motion effects and costs, in addition to improving the tracking of the reference G-acceleration vectors. Arm length has an inverse relationship with Coriolis and FHAR and a direct relationship with cost. For arm lengths larger than 8 m, the effect of arm length on the minimisation of Coriolis and FHAR reduces significantly. Seat position also influences the minimisation of Coriolis acceleration and FHAR. From the multi-objective optimisation within the study, the optimum seat position is located at 0.02 m to 0.23 m along the x-axis, -0.09 m to -0.25 m along the y-axis, and -0.8 m to -0.95 m along the z-axis with respect to the gondola Centre of Rotation. For the optimised arm length of approximately 8 m, the gondola requires roll rotation ranging from -90 to 50 degrees, pitch rotation ranging from -2 to 90 degrees, and yaw rotation ranging from -30 to 90 degrees. Through implementation of the optimised configurational design parameters, simulation of three ACMs was achieved in a four-DoF HCS with a maximum Root Mean Square (RMS) tracking error of 0.047 G. Coriolis and FHAR were minimised to an RMS error of 0.0216 G and 0.0185 from the desired values of 0 G and a ratio value of 1 , respectively.

Author Contributions: Conceptualization, A.W., N.M. and S.M.; methodology, A.W. and N.M.; software, A.W.; validation, A.W., N.M. and D.N.; formal analysis, A.W. and N.M.; investigation, A.W.; resources, N.M. and S.M.; data curation, A.W. and N.M.; writing—original draft preparation, A.W.; writing—review and editing, N.M., D.N. and S.M.; visualization, A.W. and N.M.; supervision, N.M., D.N. and S.M.; project administration, N.M. All authors have read and agreed to the published version of the manuscript.

Funding: This research received no external funding.

Data Availability Statement: The data presented in this study are available on request from the corresponding author.

Conflicts of Interest: The authors declare no conflict of interest.

References

1. North Atlantic Treaty Organization (NATO); Advisory Group for Aerospace Research and Development (AGARD). *Aerospace Medical Panel Working Group 14. High G Physiological Protection Training*; AGARDograph, No. 322; AGARD: Neuilly-sur-Seine, France, 1990.
2. AFMAN 11-403; Aerospace Physiological Training Program. United States Air Force: Washington, DC, USA, 2020. Available online: https://static.e-publishing.af.mil/production/1/af_a3/publication/afman11-403/afman11-403.pdf (accessed on 1 December 2021).
3. Chiang, K.T.; Tu, M.Y.; Lin, Y.J.; Hsin, Y.H.; Chiu, Y.L.; Li, F.L.; Chen, H.H.; Lai, C.Y. A Cardiac Force Index Applied to the G Tolerance Test and Surveillance among Male Military Aircrew. *Int. J. Environ. Res. Public Health* **2021**, *18*, 8832. [CrossRef]
4. Environmental Tectonics Corporation. About ETC. Available online: <https://www.etcaircrewtraining.com/about.html> (accessed on 13 October 2023).
5. AMST-Systemtechnik GmbH. HTC Human Training Centrifuge. Available online: <https://www.amst.co.at/en/aerospace-medicine/training-simulation-products/human-training-centrifuge/> (accessed on 12 October 2023).
6. Mohajer, N.; Najdovski, Z.; Nahavandi, S. An Efficient Design Solution for a Low-Cost High-G Centrifuge System. *IEEE/ASME Trans. Mechatron.* **2020**, *26*, 134–145. [CrossRef]
7. Mohajer, N.; Nahavandi, D.; Watson, M.; Nahavandi, S. Motion and Dynamic Analyses of a Human Centrifuge System with an Efficient Design Configuration. *Aerosp. Sci. Technol.* **2021**, *117*, 106972. [CrossRef]
8. North Atlantic Treaty Organization (NATO). *Minimum Requirements for Physiological Training of Aircrew in High “G” Environment*; NATO Standardization Office: Brussels, Belgium, 2017.
9. Winter, A.; Mohajer, N.; Nahavandi, D. Simulation of aircraft multi-axis acceleration in a four-axis Human Centrifuge System. *Aerosp. Sci. Technol.* **2023**, *140*, 108486. [CrossRef]
10. ATFS-400-31; Human Centrifuge. Environmental Tectonics Corporation: Southampton, PA, USA, 2021. Available online: <https://www.etcaircrewtraining.com/atfs-400-31-high-g-human-centrifuge-tactical-trainer.html> (accessed on 8 July 2021).

11. ATFS-400-25; Human Centrifuge. Environmental Tectonics Corporation: Southampton, PA, USA, 2021. Available online: <https://www.etcaircrewtraining.com/afcs-400-25-high-g-human-centrifuge-tactical-trainer.html> (accessed on 8 July 2021).
12. Mkhoyan, T.; Wentink, M.; Van Paassen, M.M.; Mulder, M.; de Graaf, B. Mitigating the Coriolis Effect in Human Centrifuges by coherent G-misalignment. In Proceedings of the AIAA Scitech 2019 Forum, San Diego, CA, USA, 7–11 January 2019. [CrossRef]
13. Vidakovic, J.; Lazarevic, M.; Kvrđic, V.; Vasovic Maksimovic, I.; Rakic, A. Flight Simulation Training Devices: Application, Classification, and Research. *Int. J. Aeronaut. Space Sci.* **2021**, *22*, 874–885. [CrossRef]
14. Kvrđic, V.M.; Vidakovic, J.Z.; Lutovac, M.M.; Ferenc, G.Z.; Cvijanovic, V.B. A control algorithm for a centrifuge motion simulator. *Robot. Comput.-Integr. Manuf.* **2014**, *30*, 399–412. [CrossRef]
15. Smrz, V.; Boril, J.; Leuchter, J.; Blasch, E. Experience with objective measuring of the coriolis illusion influence on the pilot's spatial orientation. In Proceedings of the 2017 IEEE/AIAA 36th Digital Avionics Systems Conference (DASC), St. Petersburg, FL, USA, 17–21 September 2017; pp. 1–6.
16. Krishnaswamy, P.B.; Fegley, K.A. Reducing Undesirable Effects in the Human Centrifuge. *IEEE Trans. Aerosp. Electron. Syst.* **1965**, *AES-1*, 29–38. [CrossRef]
17. Newman, D.G. *High G Flight: Physiological Effects and Countermeasures*; Routledge: London, UK, 2016.
18. Paul, M.A. Extended-coverage-bladder G-suits can provide improved G-tolerance and high Gz foot pain. *Aviat. Space Environ. Med.* **1996**, *67*, 253–255. [PubMed]
19. Green, N.D.C.; Brown, M.D.; Coote, J.H. Failure of vascular autoregulation in the upper limb with increased +Gz acceleration. *Eur. J. Appl. Physiol.* **2007**, *100*, 621–626. [CrossRef] [PubMed]
20. McCloskey, K.; Tripp, L.; Repperger, D.; Popper, S. Subjective reports concerning assisted positive pressure breathing under high sustained acceleration. In *High Altitude and High Acceleration Protection for Military Aircrew 6 p(SEE N 92-18972 09-52)*; AGARD: Neuilly-sur-Seine, France, 1991.
21. Green, N. Arm arterial occlusion cuffs as a means of alleviating high+ Gz-associated arm pain. *Aviat. Space Environ. Med.* **1997**, *68*, 715–721.
22. Glaser, E.; Gunga, H.-C.; Ledderhos, C. Physiological effects and operational use of positive pressure breathing for G-protection. *Pol. J. Aviat. Med. Bioeng. Psychol.* **2017**, *22*, 18–31. [CrossRef]
23. AGARD. *Current Concepts on G-Protection Research and Development*; AGARD: Neuilly-sur-Seine, France, 1995.
24. Dourado, A.O.; Martin, C. New concept of dynamic flight simulator, Part I. *Aerosp. Sci. Technol.* **2013**, *30*, 79–82. [CrossRef]
25. Dančuo, Z.; Rašuo, B.; Kvrđić, V.; Zeljković, V. Methodology of the main drive selection for a human centrifuge. *FME Trans.* **2012**, *40*, 69–74.
26. Mahmoodi, A.; Kazemi, I. Optimal motion cueing algorithm for accelerating phase of manned spacecraft in human centrifuge. *Chin. J. Aeronaut.* **2020**, *33*, 1991–2001. [CrossRef]
27. Lewkowicz, R.; Kowaleczko, G. An inverse kinematic model of the human training centrifuge motion simulator. *J. Theor. Appl. Mech.* **2019**, *57*, 99–113. [CrossRef]
28. Vidaković, J.; Kvrđić, V.; Lazarević, M.; Vestnik, J.S. Control system design for a centrifuge motion simulator based on a dynamic model. *J. Mech. Eng.* **2018**, *64*, 465–474.
29. Chen, Y.C.; Repperger, D.W. A study of the kinematics, dynamics and control algorithms for a centrifuge motion simulator. *Mechatronics* **1996**, *6*, 829–852. [CrossRef]
30. Lewkowicz, R. A centrifuge-based flight simulator: Optimization of a baseline acceleration profile based on the motion sickness incidence. *Acta Astronaut.* **2019**, *164*, 23–33. [CrossRef]
31. Burton, R.R.; Meeker, L.J.; Raddin, J.H. Centrifuges for studying the effects of sustained acceleration on human physiology. *IEEE Eng. Med. Biol. Mag.* **1991**, *10*, 56–65. [CrossRef]
32. Feenstra, P.J.; Wentink, M.; Roza, Z.C.; Bles, W.; Valente Pais, A.R. Desdemona: A new driving-simulation platform. *Fahrzeugdynamik Methoden Model. Simul. Essen* **2007**.
33. Environmental Tectonics Corporation. KRAKEN. Available online: <https://www.etcaircrewtraining.com/kraken-spatial-disorientation-trainer.html> (accessed on 8 July 2021).
34. Tsai, M.H.; Shih, M.C. G-load tracking control of a centrifuge driven by servo hydraulic systems. *Proc. Inst. Mech. Eng. Part G J. Aerosp. Eng.* **2009**, *223*, 669–682. [CrossRef]
35. Seedhouse, E. *Pulling G: Human Responses to High and Low Gravity*; Springer: Berlin/Heidelberg, Germany, 2013.
36. Vidakovic, J.; Lazarevic, M.; Kvrđic, V.; Dančuo, Z.; Lutovac, M. Comparison of numerical simulation models for open loop flight simulations in the human centrifuge. *PAMM* **2013**, *13*, 485–486. [CrossRef]
37. Vidakovic, J.; Ferenc, G.; Lutovac, M.; Kvrđic, V. Development and implementation of an algorithm for calculating angular velocity of main arm of human centrifuge. In Proceedings of the 15th International Power Electronics and Motion Control Conference, Novi Sad, Serbia, 4–6 September 2012. [CrossRef]
38. Yu, X.; Gao, X.; Wang, L.; Wang, X.; Ding, Y.; Lu, C.; Zhang, S. Cooperative Multi-UAV Task Assignment in Cross-Regional Joint Operations Considering Ammunition Inventory. *Drones* **2022**, *6*, 77. [CrossRef]
39. Gupta, S.; Tiwari, R.; Nair, S.B. Multi-objective design optimisation of rolling bearings using genetic algorithms. *Mech. Mach. Theory* **2007**, *42*, 1418–1443. [CrossRef]
40. Wu, J.; Azarm, S. Metrics for Quality Assessment of a Multiobjective Design Optimization Solution Set. *AMSE J. Mech. Des.* **2000**, *123*, 18–25. [CrossRef]

41. Sigurdarson, N.S.; Eifler, T.; Ebro, M.; Papalambros, P.Y. Multiobjective Monotonicity Analysis: Pareto Set Dependency and Trade-Offs Causality in Configuration Design. *AMSE J. Mech. Des.* **2021**, *144*, 031704. [[CrossRef](#)]
42. Pancratz, D.J.; Bomar, J.B., Jr.; Raddin, J.H., Jr. *Modeling Platform Dynamics and Physiological Response to Short Arm Centrifugation*; F41 624-93-C-6011; Biodynamic Research Corp.: San Antonio, TX, USA, 1994.
43. De Graaf, B.; Bos, J.; Groen, E.; Tielemans, W.; Rameckers, F. *Otolith Responses during Centrifugation along Three Axes of Orientation*; Naval Aerospace Medical Research Lab: Pensacola, FL, USA, 1998.
44. Environmental Tectonics Corporation. G-LAB. Available online: <https://www.etcaircrewtraining.com/g-lab-basic-human-centrifuge.html> (accessed on 12 October 2023).
45. Environmental Tectonics Corporation. GYROLAB GL-4000. Available online: <https://www.etcaircrewtraining.com/gyrolab-4000-spatial-disorientation-trainer.html> (accessed on 8 July 2021).
46. Environmental Tectonics Corporation. KRAKEN: Disorientation Research and Training Device. Available online: <https://www.etcaircrewtraining.com/assets/datasheets/kraken.pdf> (accessed on 8 July 2021).
47. Desdemona, B.V. Desdemona—Motion Simulation for Your Proficiency. Available online: <https://desdemona.eu/> (accessed on 12 October 2023).
48. Daiker, R.; Ballard, K.; Ellis, K.K. Evaluation of low cost, user-centered alerting devices for the mitigation of flight crew spatial disorientation. In Proceedings of the AIAA Scitech 2020 Forum, Orlando, FL, USA, 6–10 January 2020; p. 0411.
49. Burns, J.W.; Ivan, D.J.; Stern, C.H.; Patterson, J.C.; Johnson, P.C.; Drew, W.E.; Yates, J.T. Protection to +12 Gz. *Aviat. Space Environ. Med.* **2001**, *72*, 413–421.
50. Lo, V.E.; Chao, S.-M. Investigation into the Effects of Backrest Angle and Stick Location on Female Strength. *Int. J. Environ. Res. Public Health* **2022**, *19*, 7. [[CrossRef](#)]
51. Repperger, D.W. A Study of Supermaneuverable Flight Trajectories through Motion Field Simulation of a Centrifuge Simulator. *AMSE J. Dyn. Syst.-T ASME* **1992**, *114*, 270–277. [[CrossRef](#)]
52. Repperger, D.W. The application of modern control theory to improve the quality of motion fidelity in ground based motion simulators. In Proceedings of the First IEEE Conference on Control Applications, Dayton, OH, USA, 13–16 September 1992; Volume 1, pp. 19–24. [[CrossRef](#)]
53. Sheffield, R.G. *Jet Fighter School: Air Combat Simulator Tactics and Maneuvers*; Compute: Greensboro, NC, USA, 1987.
54. Shaw, R.L. *Fighter Combat: Tactics and Maneuvering*; Naval Institute Press: Annapolis, MD, USA, 1985.
55. Mohajer, N.; Abdi, H.; Nahavandi, S. Dynamic response multiobjective optimization of road vehicle ride quality—A computational multibody system approach. *Proc. Inst. Mech. Eng. Part K J. Multi-Body Dyn.* **2017**, *231*, 316–332. [[CrossRef](#)]
56. Jenkins, T.; Atay, S.; Buckner, G.; Bryant, M. Genetic Algorithm-Based Optimal Design of a Rolling-Flying Vehicle. *AMSE J. Mech. Robot.* **2021**, *13*, 050907. [[CrossRef](#)]
57. Chapman, C.D.; Saitou, K.; Jakiela, M.J. Genetic Algorithms as an Approach to Configuration and Topology Design. *AMSE J. Mech. Des.* **1994**, *116*, 1005–1012. [[CrossRef](#)]
58. Coello, C.A.C.; Lamont, G.B.; Van Veldhuizen, D.A. *Evolutionary Algorithms for Solving Multi-Objective Problems*; Springer: Berlin/Heidelberg, Germany, 2007.
59. Fonseca, C.M.; Fleming, P.J. Multiobjective optimization and multiple constraint handling with evolutionary algorithms. I. A unified formulation. *IEEE Trans. Syst. Man Cybern.-Part A Syst. Hum.* **1998**, *28*, 26–37. [[CrossRef](#)]
60. Weaver-Rosen, J.M.; Malak, R.J., Jr. An Algorithm for Multi-Objective Efficient Parametric Optimization. *AMSE J. Mech. Des.* **2023**, *145*, 031709. [[CrossRef](#)]
61. Hazelrigg, G.A. On the Role and Use of Mathematical Models in Engineering Design. *AMSE J. Mech. Des.* **1999**, *121*, 336–341. [[CrossRef](#)]
62. Funke, L.W.; Schmiedeler, J.P.; Zhao, K. Design of Planar Multi-Degree-of-Freedom Morphing Mechanisms. *AMSE J. Mech. Robot.* **2015**, *7*, 011007. [[CrossRef](#)]
63. Zehner, G.F.; Hudson, J.A. *Body Size Accommodation in USAF Aircraft*; Sytronics, Inc.: Beavercreek, OH, USA, 2002; p. 114.

Disclaimer/Publisher’s Note: The statements, opinions and data contained in all publications are solely those of the individual author(s) and contributor(s) and not of MDPI and/or the editor(s). MDPI and/or the editor(s) disclaim responsibility for any injury to people or property resulting from any ideas, methods, instructions or products referred to in the content.